Four-wave mixing with Rydberg levels in rubidium vapor: Observation of interference fringes

W. C. Magno,[1] R. B. Prandini,[2] P. Nussenzveig,[2] and S. S. Vianna[1]
[1]*Departamento de Física, Universidade Federal de Pernambuco, 50670-901 Recife, PE, Brazil*
[2]*Instituto de Física, Universidade de São Paulo, Caixa Postal 66318, 05315-970 São Paulo, SP, Brazil*
(Received 31 October 2000; published 8 May 2001)

We present new results on the coherent control of a four-wave mixing signal in rubidium vapor involving Rydberg levels. By varying the relative polarizations of the laser beams responsible for the nonlinear process, we control atomic excitation routes and thus quantum interference in the medium. We observed interference fringes as a function of the relative polarizations and further developed a theoretical model based on the density-matrix formalism that is in very good agreement with our experimental results.

DOI: 10.1103/PhysRevA.63.063406 PACS number(s): 42.50.Hz, 42.65.Ky, 32.80.Rm

I. INTRODUCTION

The coherent control of the optical properties of atomic media is made possible by interference effects that are induced (or probed) by laser fields. In multilevel atomic systems, these effects are related to the observation of a variety of physical phenomena in coherent and quantum optics [1–8], and have attracted considerable interest in the application to the coherent laser control of chemical reactions [9–11]. Some studies have explored nonlinearities of the medium to observe interference between atomic polarizations that can be driven by the new fields produced in the medium itself [12–15] or induced by the incident beams. In particular, Chapple *et al.* [16] used a four-wave mixing (FWM) process to observe interference in sodium vapor, when two-photon resonances with the $5S$ and $4D$ states are driven together, by an appropriate choice of the input laser wavelengths. More recently, we observed an interference in a FWM signal, when two neighboring Rydberg states play the role of two indistinguishable quantum pathways in the system [17].

In this paper, we extend our previous experimental and theoretical results by investigating the polarization dependence of the FWM signal, using rubidium as a nonlinear medium. Briefly, interference in this system results from the existence of two or more indistinguishable quantum paths for the excitation of the atomic levels involved in the nonlinear process. Four levels are explicitly considered here: the atomic ground state, two Rydberg states almost resonant with a two-photon transition from the ground state, and an intermediate state almost resonant with a single photon stimulated emission from one of the Rydberg levels. Since all these states have internal structures (due to, at least orbital angular momentum), there are multiple quantum paths for each step of the nonlinear process. The probability amplitudes for each of these paths depend on Clebsch-Gordan coefficients, which are intimately related to the input lasers' polarizations. Hence one can manipulate almost at free will the contribution of interference terms to the FWM signal by controlling these polarizations.

The paper is organized as follows. In Sec. II we introduce our experimental system and describe how we control the lasers' polarizations. We also present the results obtained for the intensity of the FWM signal as a function of the wavelength and polarization of the incident beams. The interference effect is clearly observed. To explain the polarization dependence of the FWM signal we have developed a theoretical model, which is described in Sec. III. The analysis of our results, including the interference fringes and the comparison of experiment and theory are presented in Sec. IV, followed by our conclusions.

II. EXPERIMENTAL SYSTEM AND FOUR-WAVE MIXING SPECTRA

The experiments are carried out in a vapor cell containing both ^{85}Rb and ^{87}Rb at a pressure of 10^{-6} Torr. The cell, 5-cm long and a diameter of 3 cm, is heated up to a temperature of about 180 °C and crossed by two copropagating and linearly polarized laser beams that interact with the atomic medium. A diagram illustrating the basic experimental apparatus with the relevant rubidium energy levels is displayed in Fig. 1. One of the beams, of frequency ω_1, is produced by a pulsed dye laser with a linewidth of 0.65 cm^{-1}, pumped by the second harmonic of a neodymium doped yttrium-aluminum-garnet (Nd:YAG) laser (pulse duration 10 ns and repetition rate 5 Hz). Its wavelength is tunable around 602 nm, corresponding to two-photon transitions from the ground state $5S$ to Rydberg levels ranging from $16S$ to $19S$, and $14D$ to $17D$. For the interference effect discussed here, only levels $16D$ and $18S$ are relevant. The other beam has a fixed frequency ω_2, corresponding to the fundamental mode [infrared (IR)] of the Nd:YAG laser. This laser ($\lambda_2 = 1.064$ μm) is quasiresonant with the transition from the Rydberg levels back to the $6P_{3/2}$ level (cf. inset in Fig. 1). The two beams are focused in the middle of the cell in order to have good phase matching. The generated signal at frequency $\omega_3 = 2\omega_1 - \omega_2$ has a wavelength of approximately 420 nm and is analyzed in a monochromator and detected by a photomultiplier tube. The electronic processing of the signal is made by a boxcar and a computer. Spectra are obtained by measuring the intensity of the FWM signal as a function of the dye laser frequency.

Typical FWM spectra are presented in Fig. 2, as a function of the dye laser detuning, $\Delta_1 = 2\omega_1 - \omega_{16D}$, with respect to the two-photon transition $5S \rightarrow 16D$. The polarization of the IR laser is linear and kept fixed. For the lasers propagating along the z axis, x and y are orthogonal directions with the IR laser along the x axis. The dye laser polarization is always linear but its orientation can be rotated by an angle θ

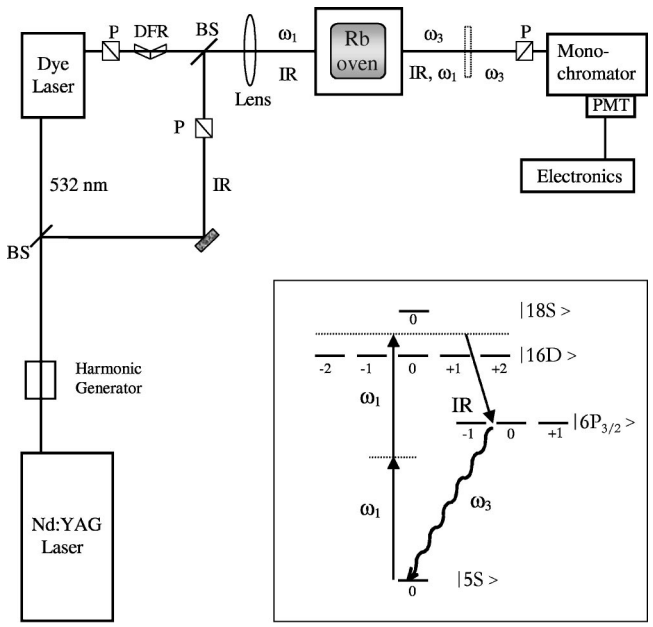

FIG. 1. Schematic diagram of the experimental apparatus. The symbols *BS*, *P*, and *DFR* stand for the beam splitter, Glan-Thompson polarizer, and double Fresnel rhomb, respectively. The inset shows the relevant rubidium energy levels, with the m_l sublevels.

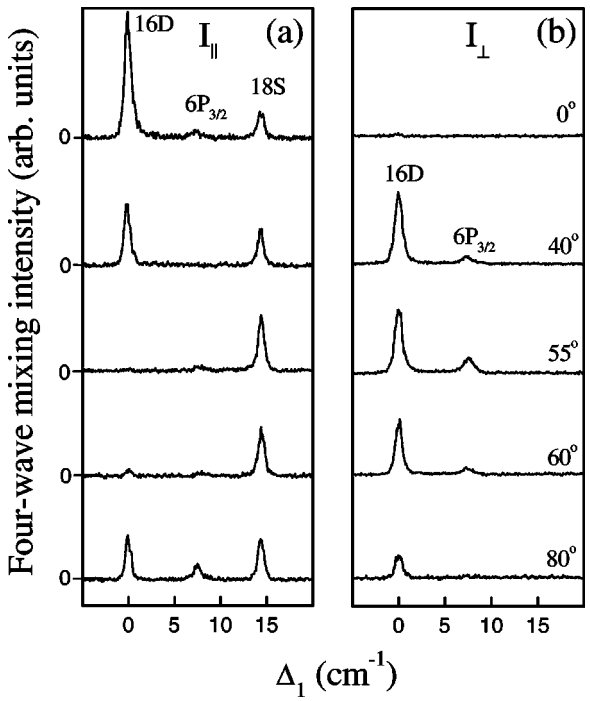

FIG. 2. FWM spectra as a function of the detuning Δ_1 of the dye laser, for several angles between the incident polarizations. The generated signal is analyzed with parallel (a) and perpendicular (b) polarization relative to the IR beam. Dye laser and IR laser intensities were $I_{dye}=5\times10^7$ W/cm^2, $I_{IR}=2.6\times10^9$ W/cm^2. The atomic density was $N=4.4\times10^{14}$ atoms/cm^3.

relative to the IR beam polarization, using a double Fresnel rhomb. At the output of the cell we can analyze the polarization of the generated signal with a Glan-Thompson polarizer. The generated signals with parallel polarization ($I_\parallel$) or perpendicular polarization ($I_\perp$) relative to the IR beam polarization are shown in Figs. 2(a) and 2(b), for some values of θ between 0° and 90°.

As in Ref. [17], we observe three peaks in each spectrum. The origin of each can be understood quite simply. The process corresponds to the absorption of two dye laser photons followed by a stimulated emission of one IR photon and a parametric emission of a photon of wavelength $\lambda_3 \approx 420$ nm. Naturally the signal is amplified each time one of the intermediate states becomes resonant with the lasers. Therefore we expect two peaks corresponding to the two-photon resonances with the levels 16*D* and 18*S* and a third peak corresponding to a three-photon resonant transition from the ground state to the $6P_{3/2}$ state.

Other features in Fig. 2 call our attention. Analyzing the component of the generated signal parallel to the IR polarization [Fig. 2(a)], we note that the 16*D* line presents a great variation with the angle between incident polarizations. In particular, for a specific angle ($\theta=55°$) the 16*D* peak disappears completely and, for $\theta=0°$ (parallel incident polarizations) a maximum intensity is observed. The $6P_{3/2}$ line also presents a dependence with the incident polarizations, while the 18*S* line is almost constant. For signal polarization perpendicular to the IR polarization [Fig. 2(b)], the 18*S* line vanishes completely, while the other lines present a dependence with the incident polarizations.

In order to fully understand all these features we have developed a theoretical model, which we describe in Sec. III.

III. THEORETICAL MODEL

The FWM signal intensity is proportional to the square of the polarization induced in the medium at the frequency $\omega_3 = 2\omega_1 - \omega_2$. The lowest order of perturbation theory that can describe this process requires us to keep terms up to second order in the dye laser field, $E_1(\omega_1)$, and first order in the IR field, $E_2(\omega_2)$. The nonlinear atomic polarization $P(\omega_3)$ along the $i(i=x,y)$ direction, is then given by (in mks units)

$$P_i^{(3)}(\omega_3)=\epsilon_o\sum_{jkl}\chi_{ijkl}^{(3)}E_{2j}^{*}(\omega_2)E_{1k}(\omega_1)E_{1l}(\omega_1), \qquad (1)$$

where the third-order susceptibility contains the microscopic informations about the atomic system. The subscripts of the nonlinear tensor $\chi_{ijkl}^{(3)}(-\omega_3;\omega_1,\omega_1,-\omega_2)$ are related with the polarization components of the incident and generated fields. For an isotropic medium, as the Rb vapor, only four elements are different from zero and, in view of the properties of group symmetry [18], they are related to each other by $\chi_{xxxx}=\chi_{xxyy}+\chi_{yxxy}+\chi_{yxyx}$. According to the experiment, we assume that the field $E_2(\omega_2)$ has a fixed polarization along the *x* axis, while the field $E_1(\omega_1)$, that drives the two-photon absorption, can have linear polarization in any direction in the *xy* plane. In this case, the generated FWM polarization will have two components, parallel (*x*) and perpendicular (*y*) to the IR beam's polarization:

$$P_x^{(3)}(\omega_3)=\epsilon_o\chi_x|E_2||E_1|^2, \qquad (2)$$

$$P_y^{(3)}(\omega_3)=\epsilon_o\chi_y|E_2||E_1|^2, \tag{3}$$

where the effective susceptibilities χ_x and χ_y are

$$\chi_x=\chi_{xxxx}\cos^2(\theta)+\chi_{xxyy}\sin^2(\theta), \tag{4}$$

$$\chi_y=(\chi_{yxxy}+\chi_{yxyx})\cos(\theta)\sin(\theta), \tag{5}$$

and θ is the angle between the polarizations of the E_1 and E_2 incident fields.

The third-order susceptibility can be calculated using the density-matrix formalism [18] applied to a four-level system. Each element of the nonlinear susceptibility contains products of four matrix elements of the electric dipole operator $\vec{Q}=e\vec{r}$, of the form $\langle nlm_l|\vec{Q}|n'l'm_l'\rangle$, which connect the initial and final atomic states through a chain of three intermediate states. For the present experiment, two neighboring Rydberg levels (16*D* and 18*S*), play the role of on or near two-photon resonant intermediate states. Thus, each nonlinear susceptibility element has a general form

$$\chi_{ijkl}=\sum_{abn}\frac{N}{\epsilon_o\hbar^3(\Delta_2-i\gamma_{ab})}\left\{\sum_c\frac{\mu_{ab}^i\mu_{bc}^j\mu_{cn}^k\mu_{na}^l}{(\Delta_1-i\gamma_{ac})(\omega_{nc}-\omega_1)}+\sum_d\frac{\mu_{ab}^i\mu_{bd}^j\mu_{dn}^k\mu_{na}^l}{(\Delta_1-\alpha-i\gamma_{ad})(\omega_{nd}-\omega_1)}\right\}, \tag{6}$$

where the subscripts *a*, *b*, *c*, and *d* stand for, respectively, the sublevels of the $5S$, $6P_{3/2}$, 16*D*, and 18*S* of the rubidium atom. These sublevels must be summed over in order to give the total contribution to the nonlinear susceptibility. The sum over odd-parity states *n* accounts for all possible intermediate states in the two-photon transition from state *a* to *c* or *d*. The $\mu_{\eta\rho}^q$ are the electric dipole matrix elements between levels η and ρ, in the direction of the applied fields, and we assume that the axis of quantization is along the direction of the propagating beams. We have defined the detunings $\Delta_1=2\omega_1-\omega_{ac}$ and $\Delta_2=(2\omega_1-\omega_2)-\omega_{ab}$, and introduced as well the relaxation rates γ_{ab}, γ_{ac}, and γ_{ad}. The quantity $\alpha\approx 14.4$ cm^{-1} is the separation between the 16*D* and 18*S* Rydberg levels and the atomic density is given by N (atoms/m^3).

The electric dipole matrix elements can be factorized into two parts: one containing the angular dependence and the other that contains the radial matrix element. For this calculation we neglected the fine and hyperfine structures and the Doppler broadening, which are unresolved by the lasers in the experiment. We also consider that only the $5P$ state contributes to the two-photon transitions between the ground state and the Rydberg levels. In this case, the angular part of the matrix element is given by the Clebsh-Gordan coefficients associated to each pathway. When the 18*S* level corresponds to an intermediate state, the sum over all degenerate sublevels with different m_l contains four indistinguishable quantum paths. Considering the dependence of the phase between these pathways with the incident-beam polarizations, we obtain that the susceptibility elements satisfy the following relations: $\chi_{xxxx}=\chi_{xxyy}$ and $\chi_{yxyx}=\chi_{yxxy}=0$. If the 16*D* level is an intermediate state, the sum over the m_l sublevels contains six indistinguishable routes, which lead to $\frac{3}{4}\chi_{xxxx}=-\frac{3}{2}\chi_{xxyy}=\chi_{yxyx}=\chi_{yxxy}$. These relations only depend on the orbital angular moment, *S* or *D*, of the intermediate levels, so they are the same obtained by Yuratich and Hanna [19] and Bethune [20].

Taking into account the respective Clebsch-Gordan coefficients for each excitation route, we obtain, for the effective susceptibilities:

$$\chi_x\propto\frac{N}{(\Delta_2-i\gamma_{ab})}\left[\frac{(4/45)Rf(\theta)}{(\Delta_1-i\gamma_{ac})}+\frac{1/9}{(\Delta_1-\alpha-i\gamma_{ad})}\right], \tag{7}$$

$$\chi_y\propto\frac{N}{(\Delta_2-i\gamma_{ab})}\left[\frac{(2/15)Rg(\theta)}{(\Delta_1-i\gamma_{ac})}\right]. \tag{8}$$

Here R is the ratio between the reduced matrix elements, given by

$$R=\frac{\langle 6P|r|16D\rangle\langle 16D|r|5P\rangle}{\langle 6P|r|18S\rangle\langle 18S|r|5P\rangle}, \tag{9}$$

and the functions that describe the angular dependence with θ are

$$f(\theta)=\cos^2(\theta)-\tfrac{1}{2}\sin^2(\theta), \tag{10}$$

$$g(\theta)=\cos(\theta)\sin(\theta). \tag{11}$$

IV. RESULTS AND DISCUSSIONS

The theory developed in the last section allows us to understand the spectral features observed in Fig. 2. First let us consider the behavior of the 18*S* line. For signal polarization parallel to the IR polarization [Fig. 2(a)], the intensity of the 18*S* line is practically constant. This is in good agreement with the predictions of Eq. (7), where the term resonant with the 18*S* level ($\Delta_1=\alpha$) does not depend on θ. For the signal polarization perpendicular to the IR polarization [Fig. 2(b)], the 18*S* line vanishes completely for all angles, in agreement with Eq. (8). This behavior can also be seen from Eqs. (4) and (5), using the fact that the Clebsch-Gordan coefficients, for all quantum paths of the FWM process involving the intermediate 18*S* level, give $\chi_{xxxx}=\chi_{xxyy}$ and $\chi_{yxyx}=\chi_{yxxy}=0$. In this case, the interference is determined by the polarization relation between the two photons absorbed in the transition $5S\rightarrow 18S$, and it is independent of the dye laser polarization. Since, for the present experiment, these two photons have the same frequency, we are very far from the $5P$ resonance level ($\omega_1-\omega_{5P}\sim 3.000$ cm^{-1}) and the fine-structure splitting is negligible. For this situation, a constructive (destructive) interference is obtained when these two photons have parallel (perpendicular) polarizations, in contrast with what is observed in Ref. [21], where the single photon energy is in between the fine-structure levels ($5P_{1/2}$ and $5P_{3/2}$).

In order to analyze the intensity of the 16*D* line as a function of the angle θ, we plot this dependence in Fig. 3 for parallel and perpendicular signal polarizations. We can im-

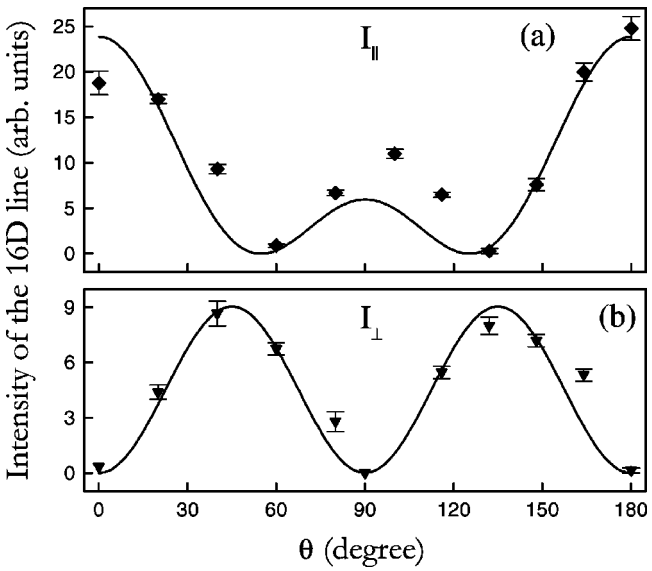

FIG. 3. Intensity of the 16*D* line as a function of the angle between the incident polarizations. The interference fringes are observed when the generated signal has parallel (a) and perpendicular (b) polarization relative to the IR beam. Solid lines are theoretical results based on Eq. (7) and Eq. (8) with the respective Clebsch-Gordan coefficients.

mediately recognize interference fringes for both polarizations. In particular, we observe that the parallel component of the 16*D* line [Fig. 3(a)] can vanish for an angle $\theta = \cos^{-1}(1/\sqrt{3})$. Fringes result from the fact that the *D* intermediate level has a degeneracy greater than one. In other words, there are multiple quantum paths for the intermediate state considered, and the Clebsch-Gordan coefficient for each quantum path depends on the polarization relation between the incident beams. So, the observed behavior of the generated signal with the polarization can be understood as an interference between the different quantum pathways, due to the several atomic sublevels m_l and the different beam polarizations. By varying the angle between the incident beam polarizations, we are able to control continuously the relative phase between the different excitation routes accessible to the system.

The solid lines in Figs. 3(a) and 3(b) represent the theoretical results of Sec. III (multiplied by a single adjustment parameter). The intensity dependence of the 16*D* line with the parameter θ is given directly by functions $f^2(\theta)$ and $g^2(\theta)$, for parallel and perpendicular signal polarizations, respectively. We consider here only orbital angular momentum but taking the fine structure into account does not change the results. We observe very good agreement between theory and experiment except for values around $\theta = 90°$ for parallel signal polarization [Fig. 3(a)]. We still do not fully understand the origin of this discrepancy. It may be related with a nonlinear absorption in the medium, in view of the fact that, for this line, the theoretical imaginary part of the susceptibility changes from negative (absorption) to positive (gain) as θ varies from 0° to 90°.

The interference ''contrast'' as a function of the angle θ, can also be measured using the quantity P_L [22] defined as

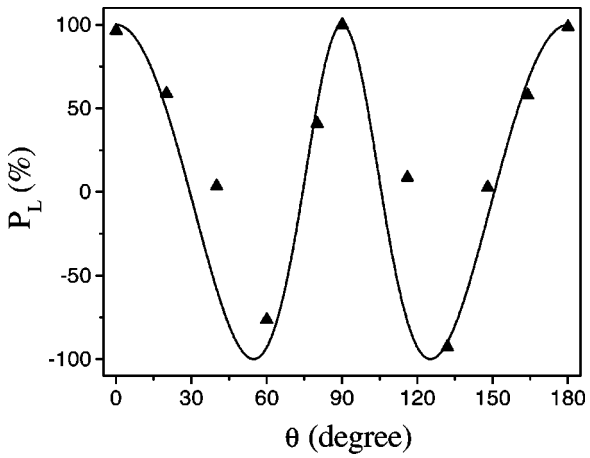

FIG. 4. The interference ''contrast'' P_L as a function of the angle θ, for the rubidium 16*D* line. The solid curve is the theoretical result based on Eqs. (7) and (8).

$$P_L(\theta) = \frac{I_{\parallel} - I_{\perp}}{I_{\parallel} + I_{\perp}}, \tag{12}$$

where $I_{\parallel}$ and $I_{\perp}$ are the FWM intensities for parallel and perpendicular signal polarizations [Figs. 3(a) and 3(b), respectively]. The experimental values of $P_L(\theta)$ for the dye laser frequency resonant with the two-photon transition $5S \rightarrow 16D$ are displayed in Fig. 4. The solid curve is the theoretical calculation obtained using expressions (7) and (8) for $\Delta_1 = 0$ (16*D* line). This result shows that for the rubidium 16*D* line it is possible to vary $P_L(\theta)$ continuously from $+100\%$ up to -100%, corresponding to maximum contrast of the interference fringes and a very efficient coherent control of the nonlinear signal.

The results obtained for the 18*S* and the 16*D* lines are quite general. For the FWM process considered here any *S* or *D* line of an arbitrary alkali atom will exhibit the same behavior with θ, since it does not depend on the specific dipole moment. In fact, we have observed the same behavior for the 15*D* and 17*S* lines in rubidium. In Fig. 5, we show the FWM spectra for these lines, as a function of the detuning of the dye laser with respect to the two-photon transition $5S \rightarrow 15D$, for three specific values of the angle between the incident polarizations ($\theta = 0°$, 55°, and 90°). Again we observed two peaks corresponding to the two-photon resonances with the levels 15*D* and 17*S* and a third peak corresponding to a three-photon resonant transition from the ground state to the $6P_{1/2}$ state. We can see that the same critical angle ($\theta = 55°$) destroys completely the FWM signal for the 15*D* line. This gives us confidence in the validity of our model but does not allow one to obtain specific information about the system.

Information about the system can be obtained by turning our attention back to the interference observed on the $6P_{3/2}$ line. Recalling the results from Ref. [17], this line depends on the excitation via 18*S* and 16*D* levels. Since the intensities of these lines vary as a function of the angle θ, it is more reasonable to study a relative intensity. We weigh the $6P_{3/2}$ line intensity by the sum of the intensities of the 16*D* and 18*S* lines. Since the 18*S* line vanishes for signal polarization perpendicular to the IR polarization, we analyze only the

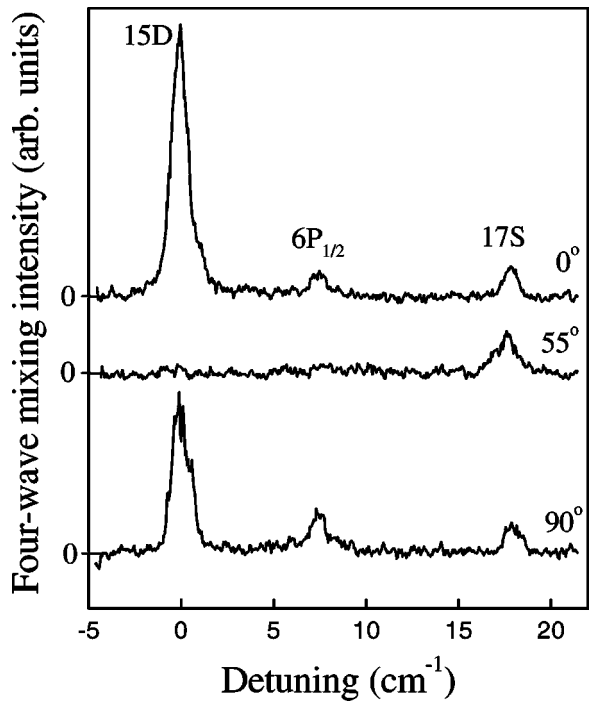

FIG. 5. FWM spectra for $6P_{1/2}$, 15*D*, and 17*S* rubidium lines, as a function of the detuning of the dye laser, for a few angles between the incident polarizations. The generated signal is analyzed with parallel polarization relative to the IR beam.

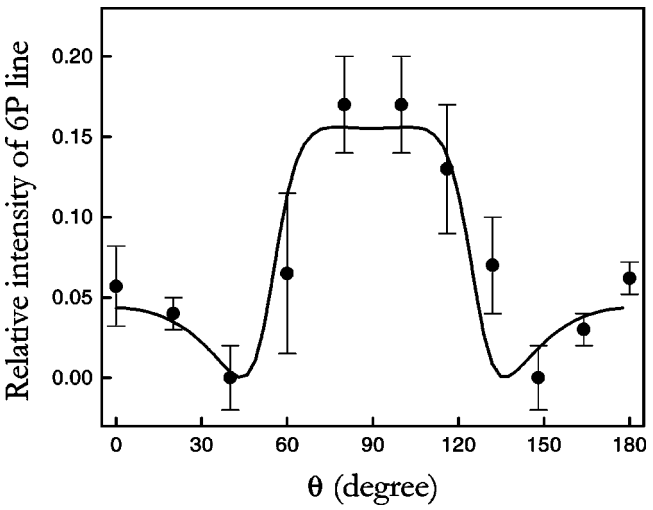

FIG. 6. Relative intensity of the $6P_{3/2}$ line as a function of the angle between the incident polarizations. The interference fringe is observed when the generated signal has parallel polarization relative to the IR beam. The solid line is a theoretical fit based on Eq. (7).

parallel polarization component of the FWM signal. The experimental results are plotted in Fig. 6. The solid line corresponds to the theoretical curve of the relative intensity of the $6P_{3/2}$ line, calculated from the maximum intensity of each line, for different values of θ. For this, we first do a theoretical fit of the FWM spectra showed in Fig. 2(a). We consider that the rate γ_{ab} is given by the half-width of the $6P_{3/2}$ line ($\approx 0.7\ \mathrm{cm}^{-1}$), which is limited by the linewidth of the IR beam. The free parameters in this fit are the relaxation rates γ_{ac} and γ_{ad} of the Rydberg levels. The value of the ratio between the reduced radial matrix elements [Eq. (9)], $R = 4.2$, is obtained by a numerical calculation using a method based on the diagonalization of the energy matrix [23]. To take into account the finite linewidth of the dye laser ($\delta_1 = 0.65\ \mathrm{cm}^{-1}$), we perform a convolution with its measured Gaussian line shape. The theoretical curves are then obtained by numerical integration of Eq. (7). The best fit of the FWM spectra give $\gamma_{ac} = 0.130 \pm 0.004\ \mathrm{cm}^{-1}$ and $\gamma_{ad} = 0.090 \pm 0.005\ \mathrm{cm}^{-1}$, in agreement with Ref. [17]. Although the values of γ_{ac} and γ_{ad} are smaller than the laser linewidth, they are basically determined by the intensity relation between the observed lines (see the Appendix). The fit is made only for one polarization, $\theta = 90°$, where all three peaks have comparable intensities, and the same parameters are used for all the values of θ. A good agreement between theory and experiment is observed. We obtain a constructive interference in the region around $\theta = 90°$ and a completely destructive interference for $\theta = 43°$. This maximum of the destructive intereference is determinated by the conditions $\Delta_2 = 0$ and $\Delta_1/(\Delta_1 - \alpha) = -\frac{4}{5} R f(\theta)$, where the factor $(\frac{4}{5})$ comes from the Clebsh-Gordan coefficients. In this case, the polarization relation between the incident fields is responsible for a three-photon transparency, similar to the previously reported two-photon transparency in two color experiments in sodium [24].

V. CONCLUSIONS

In this paper new experimental results were reported on the dependence of the FWM signal with the relative polarizations of the incident (IR and dye) laser beams. Interference effects were observed for the 16*D*, 18*S*, and $6P_{3/2}$ rubidium levels, where the different quantum pathways lead to distinct behaviors. For the 18*S* line, the interfering pathways do not change with the dye laser polarization. So, only a completely destructive or constructive interference could be obtained. However, interference fringes were observed for the 16*D* line. In this case, the different quantum pathways are due to the several atomic sublevels and the different beam polarizations, in such a way that we are able to control continuously the relative phases between the different excitation routes accessible to the system. Moreover, the 16*D* and 18*S* Rydberg levels contribute as near two-photon resonant intermediate states for the FWM signal corresponding to the $6P_{3/2}$ line. Again, interference fringes were observed and information about the parameters of the system could be obtained. The present results show it to be possible to obtain a maximum contrast of the interference fringes and a very efficient coherent control of the nonlinear signal. A simple-theoretical model, taking into account the lasers' polarizations gives a good description of the experimental results.

ACKNOWLEDGMENTS

The authors acknowledge very useful discussions with J. W. R. Tabosa and D. Kleppner. This work was supported by CNPq, CAPES, PRONEX, and FAPESP (Brazilian Agencies).

APPENDIX

The intensity of the FWM signal is calculated from the convolution between the atomic line shape and the spectral profile of the dye laser and it can be written as

$$I_{FWM}(\tilde{\Delta}_1)=\int_{-\infty}^{\infty} I(\Delta_1)g(\Delta_1-\tilde{\Delta}_1)d\Delta_1, \tag{A1}$$

where $g(\Delta_1-\tilde{\Delta}_1)$ is given by a Gaussian function:

$$g(\Delta_1-\tilde{\Delta}_1)=\frac{1}{\sqrt{\pi}\delta_1}\exp\left[\frac{-2(\Delta_1-\tilde{\Delta}_1)^2}{\delta_1^2}\right], \tag{A2}$$

and $I(\Delta_1)$ corresponds to the atomic line shape given in Eqs. (7) and (8) as

$$I_{\parallel}\propto\frac{N^2}{(\gamma_{ab}^2+\Delta_2^2)}\left\{\frac{(1/9)^2}{[\gamma_{ad}^2+(\Delta_1-\alpha)^2]}+\frac{(4/45)^2R^2f^2(\theta)}{(\gamma_{ac}^2+\Delta_1^2)}+\frac{2(1/9)(4/45)Rf(\theta)[\gamma_{ad}\gamma_{ac}+\Delta_1(\Delta_1-\alpha)]}{[\gamma_{ad}^2+(\Delta_1-\alpha)^2][\gamma_{ac}^2+\Delta_1^2]}\right\}, \tag{A3}$$

$$I_{\perp}\propto\frac{N^2}{(\gamma_{ab}^2+\Delta_2^2)}\left[\frac{(2/15)^2g^2(\theta)}{(\gamma_{ac}^2+\Delta_1^2)}\right]. \tag{A4}$$

The resulting intensity is a Voigt profile, i.e., the convolution between Gaussian and Lorentzian profiles.

The interferometric term in Eq. (A3), for the 16*D* and 18*S* resonant frequencies, is negligible. So, for the 16*D* peak intensity, we have

$$I_{16D}(\tilde{\Delta}_1=0)\propto\frac{1}{(\gamma_{ab}^2+\Delta_2^2)\delta_1}\int_{-\infty}^{\infty}\frac{\exp[-2(\Delta_1)^2/\delta_1^2]}{(\gamma_{ac}^2+\Delta_1^2)}d\Delta_1, \tag{A5}$$

where the Lorentzian function involving the relaxation rate (γ_{ab}) of the intermediate $6P_{3/2}$ state was taken outside of the integral, since it is larger than the laser linewidth in the convolution ($\gamma_{ab}>\delta_1$). The final integral is known and involves the error function $\Phi(x)$ [25]:

$$\int_0^{\infty}\frac{e^{-\mu^2t^2}}{\beta^2+t^2}dt=\frac{\pi}{2\beta}e^{\beta^2\mu^2}[1-\Phi(\beta\mu)], \tag{A6}$$

where $x=\beta\mu=\sqrt{2}\gamma_{ac}/\delta_1$, is the relevant parameter in the determination of the peak intensity for the Rydberg levels. The intensity for 18*S* peak is similar to Eq. (A5).

[1] A. S. Zibrov, M. D. Lukin, L. Hollberg, D. E. Nikonov, M. O. Scully, H. G. Robinson, and V. L. Velichansky, Phys. Rev. Lett. **76**, 3935 (1996).
[2] F. Wang, C. Chen, and D. S. Elliott, Phys. Rev. Lett. **77**, 2416 (1996).
[3] G. S. Agarwal, Phys. Rev. A **55**, 2467 (1997).
[4] H. Lee, P. Polynkin, M. O. Scully, and S. Y. Zhu, Phys. Rev. A **55**, 4454 (1997).
[5] Fu-li Li and Shi-Yao Zhu, Phys. Rev. A **59**, 2330 (1999).
[6] E. Paspalakis, N. J. Kylstra, and P. L. Knight, Phys. Rev. Lett. **82**, 2079 (1999).
[7] R. van Leeuwen, M. L. Bajema, and R. R. Jones, Phys. Rev. Lett. **82**, 2852 (1999).
[8] D. Meshulach and Y. Silberberg, Phys. Rev. A **60**, 1287 (1999).
[9] D. J. Gauthier, J. Chem. Phys. **99**, 1618 (1993).
[10] P. Brumer and M. Shapiro, Sci. Am. **272**, 34 (1995).
[11] R. N. Zare, Science **279**, 1875 (1998).
[12] R. W. Boyd, M. S. Malcuit, D. J. Gauthier, and K. Rzazewski, Phys. Rev. A **35**, 1648 (1987).
[13] Lu Deng, W. R. Garrett, M. G. Payne, and D. Z. Lee, Phys. Rev. A **54**, 4218 (1996).
[14] O. K. Andersen, D. Lenstra, and S. Stolte, Phys. Rev. A **60**, 1672 (1999).
[15] C. Dorman, I. Kucukkara, and J. P. Marangos, Phys. Rev. A **61**, 013802 (2000).
[16] P. B. Chapple, K. G. H. Baldwin, and H. A. Bachor, J. Opt. Soc. Am. B **6**, 180 (1989).
[17] S. S. Vianna, P. Nussenzveig, W. C. Magno, and J. W. R. Tabosa, Phys. Rev. A **58**, 3000 (1998).
[18] Y. R. Shen, *The Principles of Nonlinear Optics* (Wiley, New York, 1980).
[19] M. A. Yuratich and D. C. Hanna, J. Phys. B **6**, 180 (1989).
[20] D. S. Bethune, Phys. Rev. A **23**, 3139 (1981).
[21] A. I. Beger, M. D. Havey, and R. P. Meyer, Phys. Rev. A **55**, 3780 (1997).
[22] D. Zei, R. N. Compton, J. A. D. Stockdale, and M. S. Pindzola, Phys. Rev. A **40**, 5044 (1989).
[23] M. L. Zimmerman, M. G. Littman, M. M. Kash, and D. Kleppner, Phys. Rev. A **20**, 2251 (1979).
[24] J. E. Bjorkholm and P. E. Liao, Phys. Rev. Lett. **33**, 128 (1974).
[25] I. S. Gradshteyn and I. M. Ryzhik, *Table of Integrals, Series and Products* (Academic, New York, 1965).